Nat. Hazards Earth Syst. Sci., 17, 627–639, 2017
www.nat-hazards-earth-syst-sci.net/17/627/2017/
doi:10.5194/nhess-17-627-2017

Natural Hazards and Earth System Sciences
Open Access
EGU

Coseismic displacements of the 14 November 2016 M_w 7.8 Kaikoura, New Zealand, earthquake using the Planet optical cubesat constellation

Andreas Kääb[1], **Bas Altena**[1], **and Joseph Mascaro**[2]

[1]Department of Geosciences, University of Oslo, Oslo, 0316, Norway
[2]Planet, San Francisco, 94103, USA

Correspondence to: Andreas Kääb (kaeaeb@geo.uio.no)

Received: 20 January 2017 – Discussion started: 27 January 2017
Accepted: 11 April 2017 – Published: 9 May 2017

Abstract. Satellite measurements of coseismic displacements are typically based on synthetic aperture radar (SAR) interferometry or amplitude tracking, or based on optical data such as from Landsat, Sentinel-2, SPOT, ASTER, very high-resolution satellites, or air photos. Here, we evaluate a new class of optical satellite images for this purpose – data from cubesats. More specific, we investigate the PlanetScope cubesat constellation for horizontal surface displacements by the 14 November 2016 M_w 7.8 Kaikoura, New Zealand, earthquake. Single PlanetScope scenes are 2–4 m-resolution visible and near-infrared frame images of approximately 20–30 km × 9–15 km in size, acquired in continuous sequence along an orbit of approximately 375–475 km height. From single scenes or mosaics from before and after the earthquake, we observe surface displacements of up to almost 10 m and estimate matching accuracies from PlanetScope data between ±0.25 and ±0.7 pixels (∼ ±0.75 to ±2.0 m), depending on time interval and image product type. Thereby, the most optimistic accuracy estimate of ±0.25 pixels might actually be typical for the final, sun-synchronous, and near-polar-orbit PlanetScope constellation when unrectified data are used for matching. This accuracy, the daily revisit anticipated for the PlanetScope constellation for the entire land surface of Earth, and a number of other features, together offer new possibilities for investigating coseismic and other Earth surface displacements and managing related hazards and disasters, and complement existing SAR and optical methods. For comparison and for a better regional overview we also match the coseismic displacements by the 2016 Kaikoura earthquake using Landsat 8 and Sentinel-2 data.

1 Introduction

Coseismic displacements are typically measured from satellite synthetic aperture radar (SAR) data using radar interferometry or radar tracking techniques (Massonnet and Feigl, 1998; Michel et al., 1999; Avouac et al., 2015; Kargel et al., 2016, and many others). These data and methods have the advantage of covering large areas at once (for instance, Sentinel-1 swath width is ∼ 250 km for interferometric wide swath mode), independent of cloud cover and solar illumination, and enable displacement accuracies in the range of centimetres if interferometric phase coherence is preserved. The interferometric measurements reveal the displacement component in line-of-sight from the radar satellites. Radar tracking methods measure the azimuth (flight direction of satellite) and range (line-of-sight) components of the displacements with roughly metre accuracy for entire image areas, and potentially better accuracy for selected strong artificial or natural radar reflectors (Michel and Rignot, 1999; Singleton et al., 2014; Wang and Jonsson, 2015). These methods can be combined (e.g. Fialko et al., 2001). Typical revisit times for current radar satellites are of the order of a few days to weeks (e.g. 6 days for the Sentinel-1 constellation of two satellites; 14 days for ALOS-2 PALSAR; 11 days for TerraSAR-X; 24 days for Radarsat-2).

Repeat optical satellite data are used significantly less for matching coseismic displacements due to their sensitivity to cloud cover and their reduced accuracy compared to radar interferometry. If suitable data are available, however, optical images can typically be matched with higher accuracy than radar data of similar spatial resolution because SAR data are

affected by speckle noise, which is more sensitive to ground changes than repeat optical data. Furthermore, optical data can provide a more independent displacement measurement, as radar interferometry involves phase ambiguity that can be difficult to solve when displacement gradients are large or complex.

Coseismic displacements have, for instance, been measured on repeat data from Landsat (Liu et al., 2006; Avouac et al., 2014; Barnhart et al., 2014), ASTER (Avouac et al., 2006), SPOT (Dominguez et al., 2003; Leprince et al., 2007; Konca et al., 2010), very high-resolution optical satellites (Barnhart et al., 2015; Zhou et al., 2015), or air photos (Michel and Avouac, 2006; Ayoub et al., 2009). Coseismic displacements from Sentinel-2 data have to our best knowledge not yet been published in peer-reviewed journal publications, but are used by operational services (COMET, 2016). Landsat (16 day repeat orbit, 15–30 m resolution), ASTER (16 day repeat orbit, 15 m visible and near infrared resolution) and Sentinel-2 (10 day repeat orbit, 5 day repeat orbit once the Sentinel-2A and 2B constellation is complete, 10–20 m resolution depending on band) are useful for regional displacement fields and provide the approximate horizontal motion components due to their nadir-looking geometry (only ASTER is occasionally pointed in cross-track direction). Landsat and Sentinel-2 data are provided only as orthorectified version (ASTER optionally) so that positions in these orthoimages are potentially contaminated by cross-track distortions that propagated from errors in the DEM used for orthorectification (Kääb et al., 2016; Altena and Kääb, 2017). Avouac et al. (2006) and Girod et al. (2015) demonstrated refined sensor models for ASTER that reduce georeference noise significantly, and Avouac et al. (2006) developed this approach further to enable measurement of coseismic displacements from ASTER data with an accuracy of a few metres.

Due to their high spatial resolution of up to 30 cm, repeat data from very high-resolution optical satellites such as the WorldView series or Pleiades can be used to measure coseismic displacements with centimetre to decimetre accuracy (Barnhart et al., 2015; Zhou et al., 2015). Typically, however, these satellites provide no regular acquisitions, and tasked acquisitions can be quite oblique.

Global Navigation Satellite System (GNSS) measurements provide millimetre to centimetre precise 3-dimensional displacements in a global reference system on selected points where permanent stations are running. Such high-precision point measurements can thus be highly synergistic to less precise, area-wide satellite displacement measurements, for instance by providing absolute georeference to relative satellite measurements.

In this contribution we evaluate a new class of optical satellite data to estimate coseismic displacements – optical cubesats. As a test case we investigate lateral ground displacements associated with the 14 November 2016 New Zealand earthquake. This magnitude 7.8 M_w earthquake occurred in the first few minutes of 14 November 2016 at a depth of approximately 15 km in the north-east of the South Island of New Zealand, near the town of Kaikoura, and was in terms of magnitude the second strongest earthquake in New Zealand since European settlement (GeoNET, 2016; USGS Earthquake Hazard Program, 2016). Surface motion happened mainly at the Kekerengu Fault, Papatea/Waipapa Bay Fault, Hundalee Fault, and Hope Fault, which all are part of a fault system between the Australian and Pacific plates (GeoNET, 2016) (Fig. 1). Media images from after the earthquake show significant surface ruptures at the above faults with vertical and horizontal motion clearly visible (GeoNET, 2016). A number of landslides were obviously triggered by the earthquake, and in some areas the seabed was lifted by several metres (GeoNET, 2016; Sciencealert, 2016).

In this paper we assess the potential and limitations of optical cubesats, and investigate to what extent they can complement the above-mentioned established radar and optical data and methods. For this purpose, we focus in particular on the cubesat constellation by the company Planet. First, we describe the Planet cubesat constellation and details of the image-matching methods used in this study. Next, we present the results and discuss their performance and characteristics in order to evaluate the usefulness for coseismic displacements. In the final conclusions we try to answer the research questions raised at the start of this paragraph.

2 The Planet cubesat constellation

The Planet cubesats (cubesats are sometimes also referred to as nanosatellites), called PlanetScope or more commonly "doves" and which have single cubesat series called "flocks", have a size of about 10 cm × 10 cm × 30 cm, i.e. are 3-unit cubesats (one cubesat unit is 10 cm × 10 cm × 10 cm). Their main component is a telescope and CCD area array sensor, and these are complemented by solar panels for power generation, a GNSS receiver for satellite position, a startracker for satellite orientation, reaction wheels for attitude control and stabilization, an antenna for down- and uplink, batteries, and on-board storage. One half of the 6600 × 4400 pixel CCD array acquires red–green–blue data and the other half NIR; both use a 12 bit radiometric resolution. The PlanetScope satellites provide images of about 2–4 m spatial resolution, and a size of individual scenes of roughly 20–30 km × 9–15 km (Planet Team, 2016) (Marshall and Boshuizen, 2013; Boshuizen et al., 2014; Foster et al., 2015). Ground-resolution and scene size vary with flying height and satellite version. While most other optical Earth observation instruments in space deliver images in pushbroom geometry (i.e. linear sensor arrays scanning the swath width in orbit direction), the data from the Planet satellites are frame images – an important detail with respect to systematic distortions within the image product. That is, each complete scene is taken at one single point in time, has one

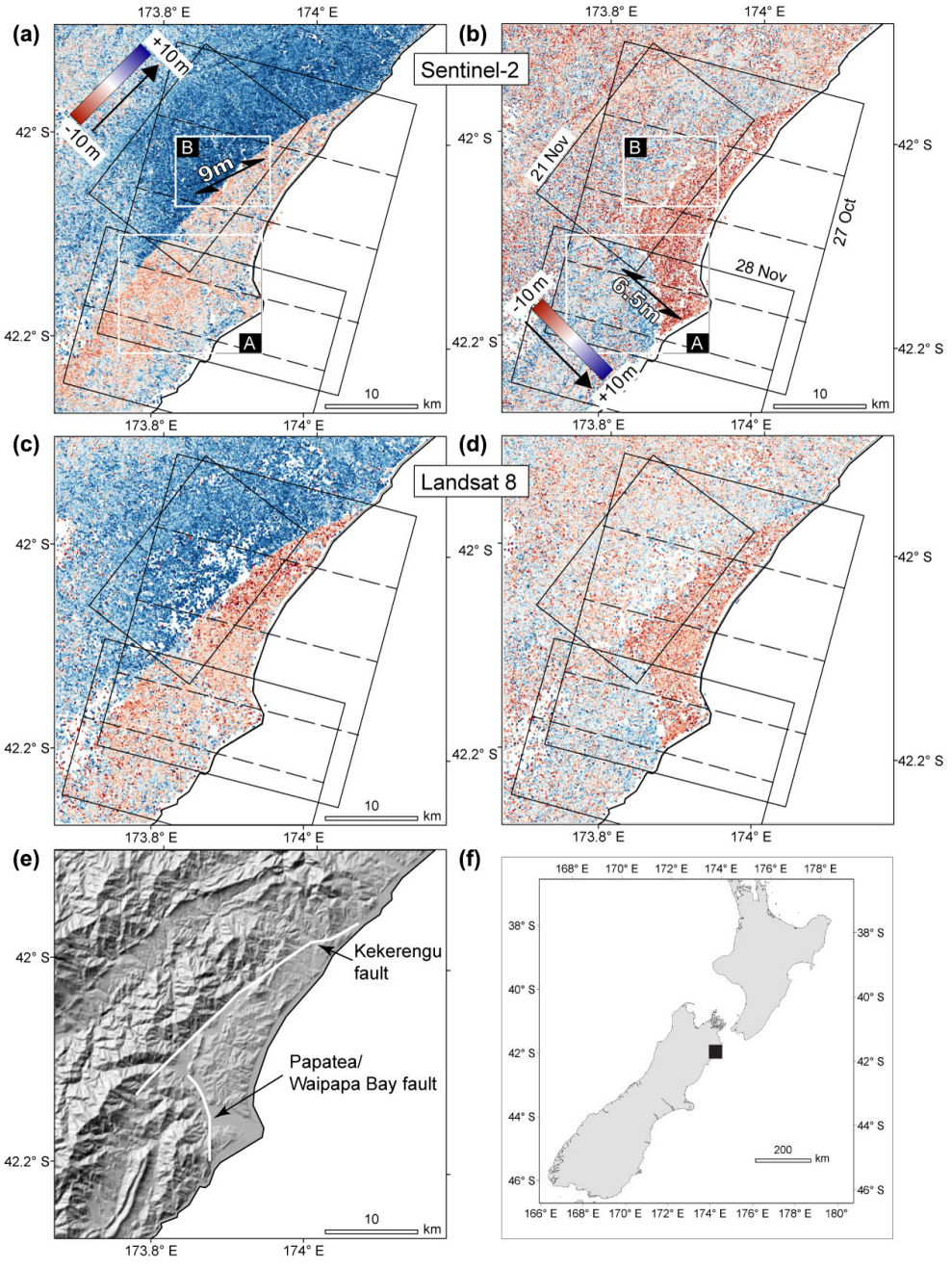

Figure 1. Sentinel-2 (3 October–5 December 2016, (**a**, **b**) and Landsat 8 (12 October–15 December 2016, (**c**, **d**) horizontal coseismic displacements of the 14 November 2016 Kaipura, New Zealand, earthquake. **(a, c)** SW–NE displacement component, **(b, d)** NW–SE component. **(e)** Hillshade from the Shuttle Radar Topography Mission (SRTM); white lines schematically indicate surface ruptures from the above displacement field. **(f)** Location of study site in New Zealand. The oblique rectangles in the upper two rows indicate the footprints of the PlanetScope images used with according dates given in **(a)**. Inset A: Fig. 3, inset B: Fig. 4.

single acquisition position and one single bundle of projection rays. For comparison, pushbroom sensors integrate an image over a certain time interval so that acquisition time, position and attitude angles vary throughout an image, which may lead to higher-order image distortions (Nuth and Kääb, 2011; Kääb et al., 2013; Girod et al., 2015).

In its final stage, the Planet cubesat constellation will consist of around 120 cubesats following each other in one near-polar orbit of 96° inclination and at an altitude of about 475 km (Fig. 2). The distance between the cubesats in this orbit is designed in a way so that the longitudinal progression between them over the rotating Earth leads to a voidless scan

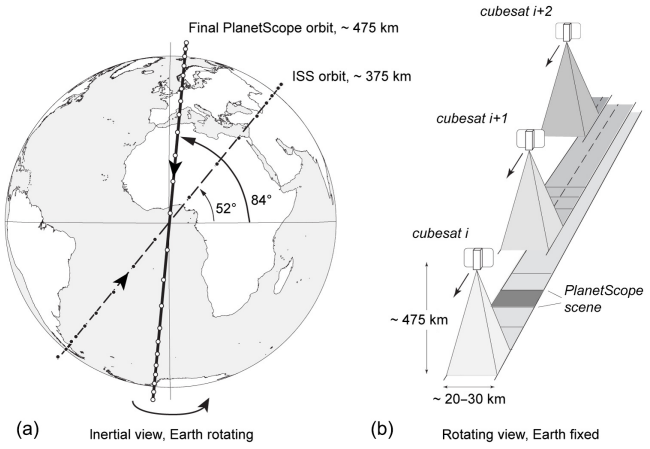

Figure 2. (a) Final PlanetScope orbit and ISS test-bed orbit. Cubesat positions (white and black dots on the orbit) are only schematically indicated. The final PlanetScope orbit is planned to host over 100 cubesats. **(b)** Scheme of complete scan of the Earth surface by successive PlanetScope cubesats (called doves) in the same orbit.

of the surface (except the polar hole) and the full constellation provides sun-synchronous coverage of the entire Earth with daily resolution (Fig. 2). At the time that the analyses were done for the present study, about 60 Planet cubesats were in space, with the majority of them not yet in a final near-polar orbit but in an International Space Station (ISS) orbit of 52° inclination and ∼ 375 km height. This preliminary constellation did not yet provide daily global coverage, and the images are taken at varying times of the day and with varying azimuths. However, 88 more PlanetScope cubesats were successfully launched on 14 February 2017 into the final sun-synchronous near-polar orbit. These cubesats should be operational within a few weeks to months after the time of writing and thus the PlanetScope constellation will be complete. We anticipate that the doves in sun-synchronous orbit will function for 3–5 years. Planet plans to keep the constellation complete by continuously supplying new satellites.

For image-matching purposes the geometric characteristics of repeat imagery is of particular interest and will thus be discussed in more detail in the following. PlanetScope images are available in different processing versions, and here we use "unrectified" and "analytic" data, both of which are accessible from Planet. "Unrectified" data come with minimal radiometric processing and are in the original frame geometry, i.e. central projection. Analytic data are radiometrically processed and orthorectified. Radiometric calibration is done through a mixture of pre-launch calibration, calibration sites, and calibration during an image coregistration process to other satellite images (the latter described below). The current lens model used during georectification was estimated once for all telescopes of the current building series and is accurate within a fraction of a pixel, better than 0.1 pixels. The image orientation parameters from on-board measurements are refined by matching the scenes onto other orthorectified images and the PlanetScope scenes are then orthoprojected using a DEM. For the first step, coregistration, Planet uses the "best available" reference images for a ground reference raster. For example, national air photo mosaics, ALOS PRISM, RapidEye, and then Landsat 8 data are preferentially used depending on which data are available and give sufficient matches. The orthorectification uses a "best available" DEM depending on location. All these processing steps and data are constantly assessed and updated, and if appropriate the archive is reprocessed.

As for all orthoprojected satellite data, vertical errors in the orthorectification DEM lead to lateral distortions in the resulting PlanetScope orthoimages, the size of which is proportional to the DEM error and the off-nadir viewing angle. For instance, for an orbit height of 400 km and a perfect nadir image of 20 km swath width (typical parameters for PlanetScope images), i.e. a maximum off-nadir distance of 10 km, a DEM error of 15 m (a typical accuracy for the SRTM DEM) (Nuth and Kääb, 2011) will translate to a maximum orthorectification distortion at the image margins of 38 cm. The Planet cubesats are controlled to acquire data within an off-nadir angle of ±2°, which, for an orbit height of 400 km, translates to a maximum off-nadir offset on the ground of 14 km in image centre and 24 km at its margin. For this maximum off-nadir viewing, the orthorectification offsets resulting from a vertical DEM error of 15 m are 52 cm in the image centre and 90 cm at the image margin. For an orbit height of 475 km and a scene width of 30 km, the latter offset numbers get 52 cm in the scene centre and 99 cm. Both scenarios represent the worst case for the propagation of orthorectification DEM errors into lateral distortions in PlanetScope images.

These expected orthorectification distortions are likely to be smaller than potential georeferencing errors from imperfect satellite positions and attitude angles, and their refinement from registering the images to reference images. Current pointing error for the satellites is of the order of 5 km prior to georectification. After georectification the georeference accuracy is 10 m RMSE according to specifications, and 6.5 m, i.e. better than the specifications, according to validation measurements by Planet. Though, at the time of writing the image referencing procedure is being upgraded.

However, distortions between unrectified frame images due to errors in image orientations are a standard problem in stereo-photogrammetry, called relative orientation. Such distortions are analytical in nature and can thus in principle be modelled and removed – in contrast to distortions from orthorectification DEM errors that are largely of unpredictable nature, depending on DEM errors. The fact that Planet images are frame images and are also available in unrectified form therefore opens in theory possibilities for own orthorectification or modelling of georeferencing errors to increase the accuracy of displacements matched from repeat images.

It should also be noted that orthorectification DEMs (or DEMs for topographic phase removal within SAR interferometry) are by necessity outdated unless acquired simultaneously with image acquisition (Stumpf et al., 2014). Any orthorectification, no matter how accurate in space, is therefore temporally corrupted by the fact that the ground is a moving target, always changing in time. Typically, ground changes will be small enough to not have a significant effect on orthorectification, but for instance for landslides, major earthquakes, or glaciers the resulting offsets are an inherent problem of orthorectification of monoscopic data (Kääb et al., 2016; Altena and Kääb, 2017). The small field of view of PlanetScope cubesats and the resulting small sensitivity to topographic distortions, the frame geometry of the PlanetScope cameras, and the accessibility of unrectified images all contribute to minimizing and potentially removing topographic distortions.

3 Data and methods

To investigate coseismic displacements from repeat optical data we match images from before and after the 14 November 2016 earthquake over the north-eastern section of the South Island of New Zealand. In order to get a regional overview of displacements we first match Sentinel-2 data of 3 October and 5 December 2016 (NIR band 8, 10 m resolution; 63 days; Copernicus, 2017), and the closest suitable Landsat 8 data around the earthquake date from 12 October and 15 December 2016 (pan band 8, 15 m resolution; 64 days; Fig. 1). For detailed displacements over the main ruptures we select PlanetScope images of 27 October, 21 and 28 November 2016 (i.e. 25 and 32-day pairs; Earthexplorer, 2017; Fig. 1). A number of other suitable Sentinel-2 and PlanetScope images are available too, but the selected ones seemed best to us in terms of illumination, cloud cover, and proximity to the earthquake date.

In order to cross-check the potential displacement accuracy from PlanetScope data, we also measured displacements from two PlanetScope scenes of 20 and 25 November 2016 just to the south-west outside of the section shown in Fig. 1. These images stem from a sun-synchronous near-polar repeat orbit as expected as standard from the final Planet constellation – and occasionally already provided at the time of writing from the preparatory constellation. No such scene from sun-synchronous near-polar orbits was available directly over the section of Fig. 1 around the earthquake date, so we use Planet scenes acquired from preliminary ISS-type orbits over the region of Fig. 1. Daily MODIS data around the earthquake date show suitable imaging conditions on 1, 3, 8 and then again on 15, 18, 19, and 21 November, etc. when the final sun-synchronous daily Planet imaging constellation would thus have had acquired data. The above test with data from sun-synchronous near-polar obits and with 5 days interval between scenes (20 and 25 November) seems thus representative and realistic.

For matching the repeat Sentinel-2, Landsat 8 and PlanetScope data we use standard normalized cross-correlation (NCC), solving the cross-correlation in the spatial domain and reaching subpixel accuracy by interpolation of the image (Kääb and Vollmer, 2000; Debella-Gilo and Kääb, 2011a; Kääb, 2014). The matching window sizes used for the Sentinel-2 data were 20×20 pixels (200 m), for Landsat 8 15×15 pixels (225 m), and for PlanetScope 20×20 pixels (60 m). Tests with different window sizes are not the focus of this study (Debella-Gilo and Kääb, 2011b). Measurements with a correlation coefficient smaller 0.7 are removed and no other postprocessing is applied. Offset patterns such as global offsets, jitter or stripes, which might have a magnitude of several metres for Landsat 8 and Sentinel-2 (Kääb et al., 2016), have not been investigated and corrected. The offsets presented here are thus relative to the matched scenes and not necessary absolute offsets in some global reference system.

Preservation of absolute georeference over the earthquake is tricky as we cannot be sure of changes in the position of the plates involved from our satellite data alone. The pointing accuracy of the satellites used is not accurate enough for that purpose and coregistration steps are involved in the processing of the Landsat and PlanetScope data in any case (and in the near future also for Sentinel-2). The focus of our evaluation therefore lies on relative displacements between scene zones. Such strain maps are also produced when (In)SAR techniques are used. Absolute georeference problems could be reduced by coregistering PlanetScope data with selected images and image sections of, for instance, Landsat 8 or Sentinel-2 data, or air photo orthoimage mosaics. Also GNSS measurements of coseismic displacements could be used to adjust the georeference of PlanetScope-derived displacements.

4 Results

4.1 Planet, Sentinel-2, and Landsat 8 coseismic displacements

Figure 1 shows the horizontal coseismic displacements from the Sentinel-2 data of 3 October and 5 December (Fig. 1, upper row), and from the Landsat 8 data of 12 October and 15 December 2016 (middle row). The main rupture by the earthquake along the Kekerengu Fault has an azimuth of roughly 45° and we thus transform the measured displacements to a Cartesian coordinate system rotated by 45°; i.e. we show the SW–NE (Fig. 1, left column) and NW–SE (right column) displacement components instead of W–E and S–N. From the repeat Sentinel-2 and Landsat 8 data the main rupture is along a sharp line over the Kekerengu Fault. There, we find relative displacements of around 9 m with an azimuth of

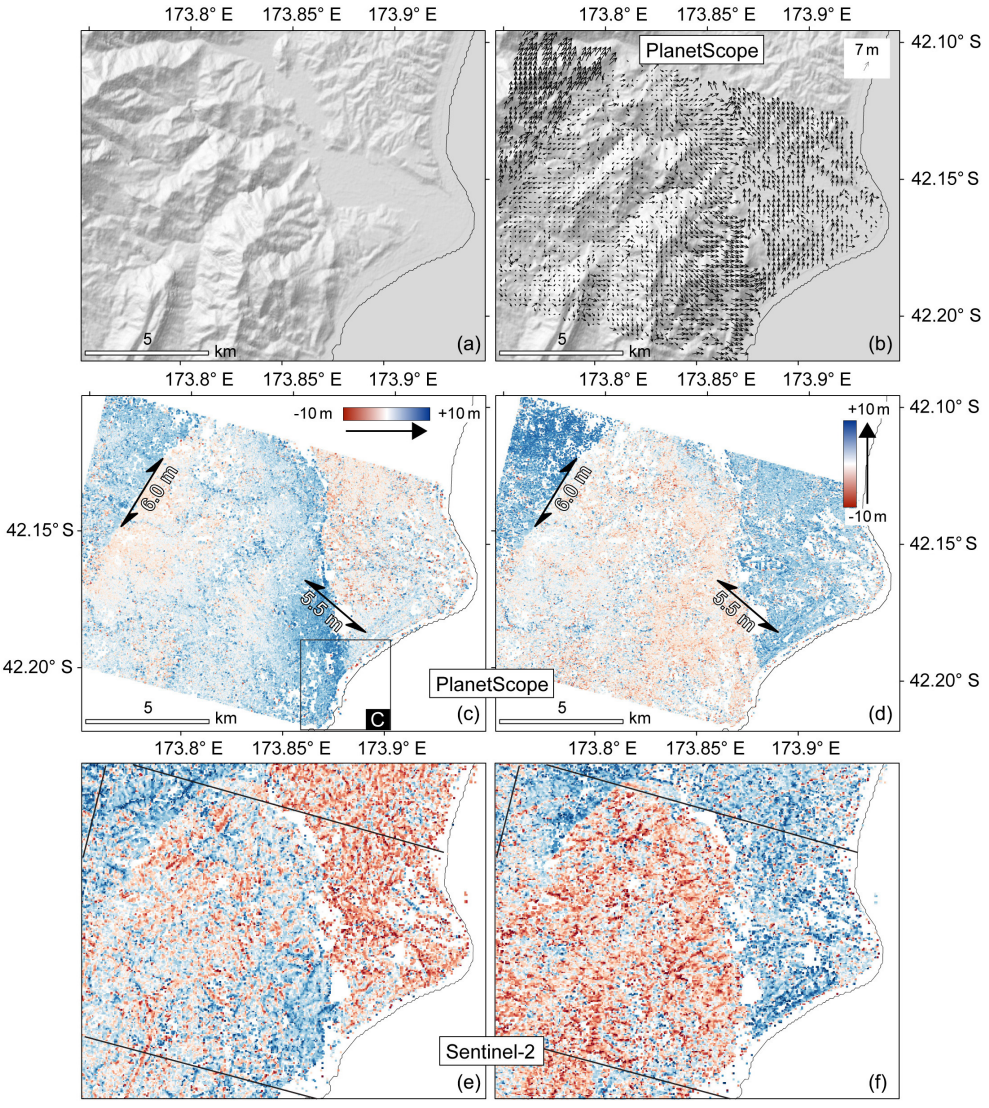

Figure 3. **(a)** Hillshade of SRTM elevation model. **(b, c, d)** Horizontal surface displacements from PlanetScope images of 27 October–28 November 2016. **(b)** Vectors measured originally with 20 m grid spacing are resampled to 200 m spacing; SRTM hillshade in background. **(c)** W–E component, **(d)** S–N component with 20 m spacing. Location of figure: A in Fig. 1. The double arrows indicate the approximate direction and the according numbers the approximate magnitude of relative displacement over ruptures. Rectangle C: Fig. 5. Lower row **(e, f)** is as middle row but displacements from Sentinel-2 data of 3 October and 5 December 2016; same colour scale.

roughly 65°. At the Papatea Fault we obtain relative displacements of around 6.5 m with an azimuth of roughly 130°.

To evaluate PlanetScope data we match a two-scene mosaic of 28 November 2016 with a mosaic of four scenes of 27 October over parts of the Kekerengu and Papatea fault ruptures (Fig. 1, rectangle A) and show the W–E and S–N components of the obtained displacements (Fig. 3, middle row). Both mosaics have been compiled from standard orthorectified PlanetScope products without any additional own corrections or adjustments. All images used for the mosaics were available with the same ground resolution so that no resampling was necessary before matching them. The measured displacements show a sharp rupture over the Kekerengu Fault of around 6 m with a rupture azimuth aligning closely with the azimuth of the displacement. Over the Papatea Fault the rupture is less straight and rather oblique to the horizontal displacement of about 5.5 m. The latter displacement agrees well within the error bounds with the Sentinel-2 results. The displacement field derived from the PlanetScope data is very dense and shows details that are not obvious from Sentinel-2 and Landsat 8; for instance the higher W–E displacements in the southernmost zone of the section in Fig. 3. Between the Kekerengu and Papatea fault ruptures in Fig. 3, we observe gradients in both the W–E and S–N displacement components resulting from an increase of displacement magnitude towards the Papatea Fault rupture and accompanied by

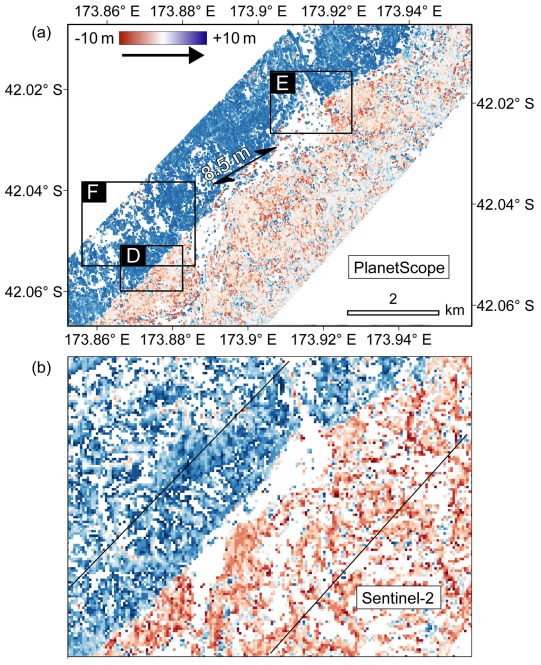

Figure 4. **(a)** Horizontal surface displacements from PlanetScope images of 27 October–21 November 2016, W–E component (S–N component is very similar). The double arrow indicates the approximate direction and the according number the approximate magnitude of relative displacement over the main rupture. Location of Figure: B in Fig. 1. Rectangle D: Fig. 6, rectangle E: Fig. 7, rectangle F: Fig. 8. **(b)** As upper panel but displacements from Sentinel-2 data of 3 October and 5 December 2016; same colour scale.

a rotation of the displacement field towards east closer to the rupture (Fig. 3, top row).

The lower row in Fig. 3 shows Sentinel-2-derived displacements for comparison, i.e. details of Fig. 1 (upper row), but with N–S and E–W displacement components.

On another section at the Kerengu Fault rupture (Fig. 1, rectangle B) we match a PlanetScope scene of 21 November with the 27 October mosaic (Fig. 4). Only the W–E components of displacements are shown, as the S–N ones look very similar. The measurements show a sharp displacement over the rupture of around 8.5 m with an azimuth that is slightly oblique to the rupture. Again, the displacement from PlanetScope data agrees well within error bounds with the Sentinel-2 results of 9 m. Over the Clarence River floodplain no measurements are possible. The lower panel in Fig. 4 shows Sentinel-2-derived displacements over the same section for comparison.

Figure 5 shows a small detail of Fig. 3 (C in Fig. 3) with the 27 October–28 November 2016 PlanetScope-derived displacements: one panel shows 27 October and the other has the 28 November image in the background. At this location, the seabed was lifted up by roughly 2 m east of the rupture, which is also clearly visible in the 28 November image (GeoNET, 2016; Sciencealert, 2016). The main rupture obtained from the displacements is offset from the seabed rupture visible in the images.

Figure 6 shows a small detail of Fig. 4 with the PlanetScope image of 21 November in the background (location D in Fig. 4). Matches did not achieve correlation coefficients larger than 0.7 over the rupture itself due to high deformations and surface destruction, and are thus removed. At these places the rupture is visible in the underlying Planet image, confirming the accurate delineation of the rupture by the derived displacements.

Figure 7 (location E in Fig. 4) shows a detail of Fig. 4 with the PlanetScope images from 27 October and 21 November behind the displacements. Here, presumable vertical uplift of the terrain to the south-east, accompanying the horizontal displacements by the rupture, have dammed up Clarence River and changed its course as visible in the PlanetScope images.

Figure 8 (location F in Fig. 4) illustrates landslides due to the 14 November earthquake close to the Kekerengu Fault rupture in order to give an impression of the visual characteristics of the PlanetScope data and other uses of the data related to earthquake disaster management. To the south-east of the figure, the rupture is visible as a bright line.

4.2 Planet data stable ground test

As the Planet constellation was not yet final at the time of the 2016 New Zealand earthquake no images were available from the sun-synchronous near-polar orbit close to the earthquake date. To simulate displacement measurements based on PlanetScope data of this final constellation we match the overlap of PlanetScope images near our study site from 20 and 25 November 2016. Both scenes come from the sun-synchronous near-polar orbit (Fig. 9). The type of terrain and land cover over these scenes is very similar to the ones applied above over the ruptures. We performed three assessments, as follows.

In Figure 9b, matching the orthorectified versions of both images shows a mean offset of only 0.25 m, i.e. less than 0.1 pixels. The standard deviation of this offset, that is the variability of the individual displacements, is around 1.9 m, and the mean magnitude of the individual displacements is 1.6 m. This indicates an accuracy of individual displacements of about ± 0.6 pixels.

In Figure 9c, we use the unrectified versions of the two scenes, coregister them using a first-order polynomial (i.e. removing a global shift and approximately a rotation), and match them. Over most of the overlap we obtain a standard deviation of displacements of around 0.2–0.3 pixels (~ 0.75 m). Towards the left and right margins we see distortions between the scenes of up to 5–6 pixels. These are due to the superposition of the lens and image distortions of both images, distortions that are not corrected for in the unrectified data version and not sufficiently reduced by our simple first-order polynomial coregistration. A comparison

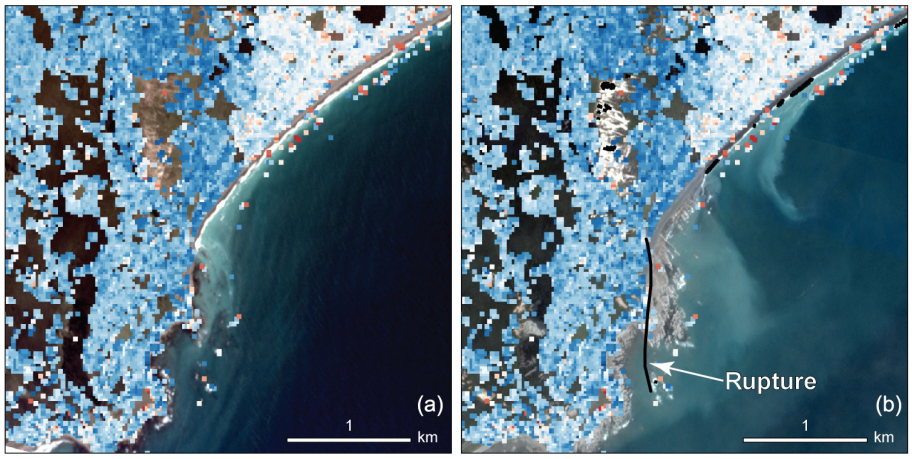

Figure 5. Horizontal surface displacements from PlanetScope images of 27 October–21 November 2016, W–E component. For colour scale see Fig. 3. **(a)** PlanetScope image of 27 October, **(b)** 21 November 2016. The section of uplifted seabed (right of the rupture) and the according rupture are visible in the PlanetScope images; the rupture is indicated by a black line that was digitized from the images. Location: C in Fig. 3.

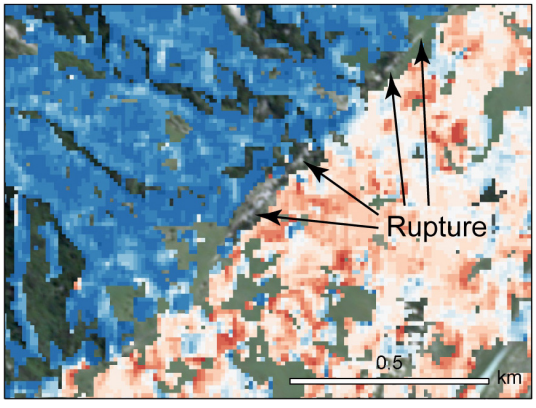

Figure 6. Horizontal surface displacements from PlanetScope images of 27 October–21 November 2016, W–E component. Background: PlanetScope image of 21 November with the surface rupture clearly visible. Location: rectangle D of Fig. 4.

with the matching based on the orthorectified images versions (Fig. 9b) shows that these effects are efficiently removed during the processing steps by Planet towards orthorectified data.

In Figure 9d, we use the same procedure as for the results Fig. 9c, but use a second-order polynomial instead, i.e. including quadratic terms in the coregistration. Now, the distortions to the right and left margins are mostly removed and a pattern of undulations of ±0.1 pixel in amplitude becomes visible. This pattern is also present in the test of Fig. 9c but is difficult to visualize there due to the overlying and much larger global scene distortion. We assume this undulating pattern is a superposition of higher-order distortions in the individual images. Again, we cannot find such pattern anymore between the orthorectified scenes. Like in the test Fig. 9c, also in Fig. 9d the standard deviation of individual displacements is of the order of 0.2–0.3 pixels.

5 Discussion

In general, the Landsat 8 and Sentinel-2 results are similar. For a number of details in the displacement field both agree, but there are also some minor differences. The latter could easily be due to imperfect coregistration within the matching pairs, or deviations/distortions of absolute georeference between the matching pairs (see end of above Sects. 2 and 3). Overall, the displacement field from the Sentinel-2 data seems slightly sharper and has fewer outliers compared to Landsat 8, as expected for the higher image resolution of Sentinel-2. For optimal ground conditions (e.g. flat desert) repeat Sentinel-2 data can be matched with an accuracy of up to 0.1–0.2 pixels (1–2 m) for single displacements (Kääb et al., 2016). From the standard deviation of displacements over homogenously displacing image sections we estimate a relative accuracy for individual displacements of about ±0.4 pixels (4 m) for Sentinel-2 and about ±0.25 pixels (3.8 m) for Landsat 8, for the matching window sizes, ground conditions and time interval specific to our study. The differences between the Sentinel-2- and Landsat-8-derived displacements are on average -0.8 ± 9.2 m in SW–NE and -1.5 ± 4.2 m in NW–SE (Sentinel-2 minus Landsat 8). The maps of differences (not shown) display a smoothly undulating pattern that could roughly be connected to topography, pointing to terrain-correction differences as a possible source of the differences between Sentinel-2 and Landsat 8 displacements (Kääb et al., 2016). Further in-depth investigations of the Sentinel-2 versus Landsat 8 differences are outside the scope of this paper.

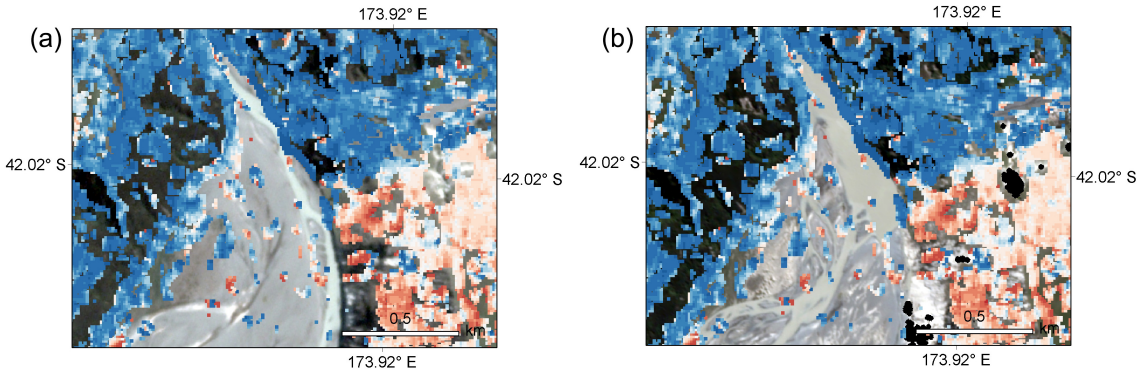

Figure 7. Horizontal surface displacements from PlanetScope images of 27 October–21 November 2016, W–E component. Background: PlanetScope images of 27 October **(a)** and 21 November **(b)**. Clarence River was dammed up by the rupture and its course was diverted. Location: rectangle E of Fig. 4.

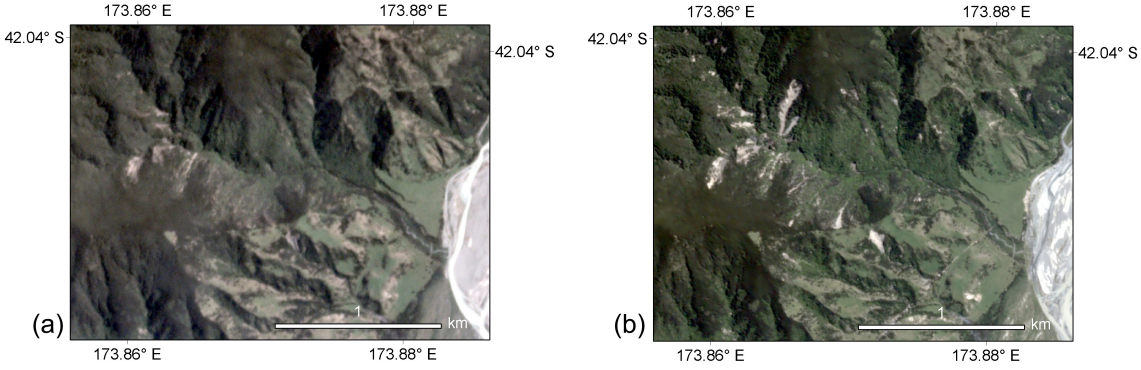

Figure 8. PlanetScope images on **(a)** 27 October, **(b)** 21 November 2016 showing landslides caused by the 14 November 2016 Kaikoura earthquake. To the lower right, the surface rupture is also clearly visible. Location: rectangle F in Fig. 4.

Whereas the overall displacement pattern between Sentinel-2 and PlanetScope agrees, the Sentinel-2 displacements show more noise and outliers (Figs. 3 and 4, lower rows), which gives in part the impression of larger displacement magnitudes. The average difference between both displacement fields is 5.3 ± 5.2 m (vector magnitude) for region A and 4.2 ± 5.2 m for region B, whereby the 5.3 or 4.2 m offsets respectively reflect the lacking and thus imperfect coregistration of both data sets. The ± 5.2 m relative uncertainty (1σ) of displacements should mainly stem from the Sentinel-2-derived ones, as Figs. 3 and 4 suggest. The difference maps between the PlanetScope and Sentinel-2 displacements for the sections of both Figs. 3 and 4 (not shown) mostly display noise but also some patterns potentially related to topography and thus orthorectification. There also seems to be some difference of the order of 2 m in overall displacement, for instance, on either side of the Papatea Fault (see Fig. 3), the reason for which is unclear (influence of shadow changes, orthorectification artefacts, or other reasons).

From the standard deviation of displacements over homogenously moving sections of the scenes used here (Figs. 3 and 4), we estimate a relative accuracy of individual displacements of about ± 0.67 pixels (2 m) for the PlanetScope data and the matching window sizes, ground conditions, and time intervals specific to our study.

Remarkably, neither in the matching between the orthorectified scenes (Figs. 3, 4, and 9b) nor between the unrectified scenes (Fig. 9c and d) do notable topographic effects become visible. This confirms that, due to the small field of view of the Planet satellites and their nadir-looking geometry, the image geometry is quite insensitive to orthorectification DEM errors or topographic distortions respectively. As a consequence, unrectified PlanetScope scenes could be used directly in a number of applications for displacement measurement without applying any topographic correction or DEM-based orthorectification.

Overall, our measurements of coseismic displacements using PlanetScope data and the test over stable ground suggest a relative accuracy of around ± 0.6–2.0 m (0.2–0.7 pixels; 1 standard deviation) for individual displacements. When averaging such displacements over defined zones, as one would typically do for investigating coseismic displacements, the accuracy (standard error) of a resulting mean zonal displacement will be significantly better than the accuracy of indi-

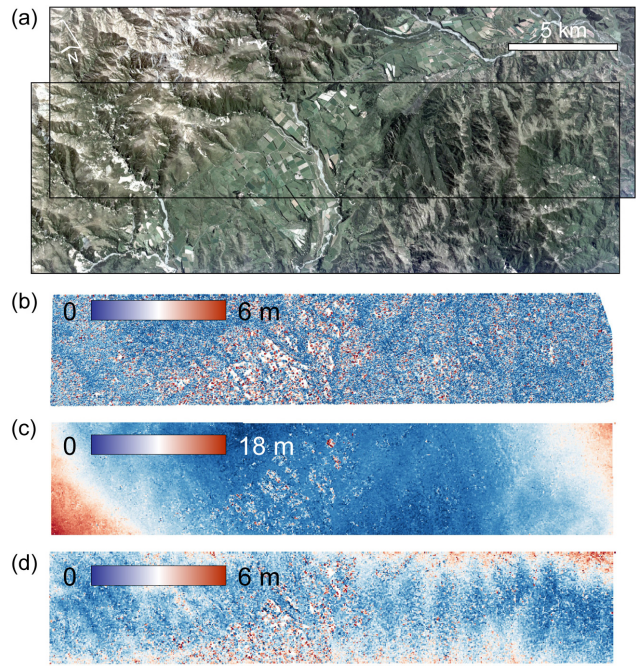

Figure 9. Horizontal surface displacements from PlanetScope images of 20–25 November 2016 without surface motion; total magnitude of displacement. **(a)** The two scenes and their overlap are matched in **(b)**–**(d)**. **(b)** Displacements between orthorectified versions. **(c)** Displacements between the unrectified versions, when coregistered using a first-order polynomial. **(d)** As in **(c)** but coregistered using a second-order polynomial.

vidual displacements (standard deviation), depending on the number of displacements averaged and their dependency on each other.

6 Conclusions

We demonstrate horizontal coseismic displacements of the 14 November 2016 Kaikoura, New Zealand, earthquake from repeat Sentinel-2, Landsat 8, and PlanetScope data. Over the two faults investigated we find horizontal surface slip of around 6–9 m. The main goal of this study was to assess the potential of PlanetScope data for this purpose.

The main limitation of optical data in general is their dependency on cloud-free conditions and solar illumination, in contrast to SAR acquisitions. Also, due to their nadir-viewing geometry most optical data give no access to the vertical component of coseismic (and other) terrain displacements. Where phase coherence is preserved within SAR radar data, displacement can be measured through interferometry by a precision that can seldom be matched by optical remote sensing data. However, where this phase coherence is not given, optical data can be a valuable alternative to radar data for coseismic (and other Earth surface) displacement measurements. The estimated displacements can also be of help to better unwrap SAR interferometry data. When the gradient of the strain increases too much, the interferometric phase fringes are difficult to follow (unwrap). However, displacements from image matching are not ambiguous so two-dimensional integration is not needed.

One of the main advantages of using PlanetScope data for coseismic displacements is their anticipated daily repeat. This maximizes the chances of receiving cloud-free images and to cover unexpected events such as earthquakes. The according small time periods of a few days that form the image-matching pairs and the related small changes in ground and illumination conditions, together with the frame geometry of the PlanetScope images, allow for relative measurement accuracies of as low as ±0.2–0.3 pixels (∼ ±0.75 m) for individual displacements and potentially much better accuracies for zonal averages. In detail, we performed three tests on this potential displacement accuracy: variance of displacements over homogenously displacing areas using orthorectified PlanetScope images from preliminary orbits (not sun-synchronous, not near polar) over actual ruptures (obtaining ±0.67 pixels); variance of displacements over stable terrain using orthorectified PlanetScope images from final orbits (sun-synchronous, near polar) with 5-day repeat (±0.63 pixels); variance of displacements over stable terrain using unrectified PlanetScope images from final orbits (sun-synchronous, near polar) with 5-day repeat (±0.2–0.3 pixels). In combination with the high spatial image resolution of around 3 m, details in the displacement field can thus become apparent that are not detected in Sentinel-2 or Landsat 8 data. The envisaged daily repeat by PlanetScope data will further improve the above displacement accuracy by enabling to measure displacements in several image pair combinations and thus exploiting a temporal stack of images and displacements (Dehecq et al., 2015; Kääb et al., 2016; Altena and Kääb, 2017; Stumpf et al., 2017).

In comparison to Sentinel-2 and Landsat 8, the main limitation of PlanetScope scenes is their extent of only a few 100 km^2. Precise georeferencing between images before and after large-scale coseismic displacements can thus be difficult as all terrain covered by a scene might have been displaced or deformed in some way. In such cases, the data provide relative displacements over smaller areas or well-defined ruptures, i.e. strong gradients in a displacement field. Long-wavelength variations or low gradients in a displacement field will be more complicated to measure as these cannot easily be discriminated from distortions in the repeated images or their coregistration. The above problems can be in parts reduced by mosaicking longer stripes of scenes instead of using single scenes, as demonstrated in our study for the 27 October and 28 November data. Finally, the above matching accuracy of the order of ±1 m will prevent detecting small (coseismic) displacements.

Though listed above as disadvantage, the small PlanetScope scene size and the connected small field of view, together with their nadir acquisition, have on the other hand the

advantage that topographic distortions in PlanetScope data are small and the resulting orthoimages quite robust against vertical errors in the DEM used for orthorectification. This effect contributes also to the good matching results above.

Finally, even if not the main focus of this study on coseismic displacements, the visual information provided by the high resolution, daily repeat PlanetScope data can be very valuable for mapping and managing the impacts of earthquakes, such as ruptures, landslides, damming of rivers, damaged infrastructure, etc. Because the downlink network of the Planet constellation has an extensive coverage, availability of PlanetScope imagery can be of the order of only several minutes, with 75 % of imagery collected available within 24 h. The speed of image availability can aid first responders, given that the first 24 h after a disaster are the most critical for saving lives.

To summarize, we find that PlanetScope data will seldom be able to completely replace more traditional satellite data for mapping coseismic displacements such as synthetic aperture radar (SAR), Landsat and Sentinel-2, or very high-resolution optical satellites, but rather complement these by filling a gap related to temporal and spatial resolution.

Code availability. The image matching code used for this study (Correlation Image AnalysiS, CIAS) is available from http://www.mn.uio.no/icemass.

Data availability. Sentinel-2 data are freely available from the ESA/EC Copernicus Sentinels Scientific Data Hub at https://scihub.copernicus.eu/, Landsat 8 data from USGS at http://earthexplorer.usgs.gov/. Planet data are not openly available as Planet is a commercial company. However, scientific access schemes to these data exist.

Author contributions. Andreas Kääb developed the study, did most of the analyses and wrote the paper. Bas Altena supported the analyses and edited the paper. Joseph Mascaro helped with data acquisition, technical details to the Planet constellation and data, and edited the paper.

Competing interests. Andreas Kääb and Bas Altena declare no competing interests. Joseph Mascaro is programme manager for impact initiatives at Planet. He did in no manner influence the results or conclusions of the study.

Acknowledgements. Special thanks are due to André Stumpf, a second anonymous referee, and the editor Norman Kerle for their valuable comments and efforts of reviewing and handling our paper. We also thank Seth Price from Planet for additional technical information on PlanetScope image processing. We are grateful to the providers of satellite data for this study: Planet for their cubesat data via Planet's Ambassadors Program, ESA/Copernicus for Sentinel-2 data, and USGS for Landsat 8 data. The work was funded by the European Research Council under the European Union's Seventh Framework Programme (FP/2007-2013)/ERC grant agreement no. 320816 and the ESA projects Glaciers_cci (4000109873/14/I-NB) and DUE GlobPermafrost (4000116196/15/IN-B).

Edited by: N. Kerle
Reviewed by: A. Stumpf and one anonymous referee

References

Altena, B. and Kääb, A.: Elevation change and improved velocity retrieval using orthorectified optical satellite data from different orbits, Remote Sens., 9, 300, doi:10.3390/rs9030300, 2017.

Avouac, J. P., Ayoub, F., Leprince, S., Konca, O., and Helmberger, D. V.: The 2005, M_w 7.6 Kashmir earthquake: Sub-pixel correlation of ASTER images and seismic waveforms analysis, Earth Planet. Sc. Lett., 249, 514–528, doi:10.1016/j.epsl.2006.06.025, 2006.

Avouac, J. P., Ayoub, F., Wei, S. J., Ampuero, J. P., Meng, L. S., Leprince, S., Jolivet, R., Duputel, Z., and Helmberger, D.: The 2013, M_w 7.7 Balochistan earthquake, energetic strike-slip reactivation of a thrust fault, Earth Planet. Sc. Lett., 391, 128–134, doi:10.1016/j.epsl.2014.01.036, 2014.

Avouac, J. P., Meng, L. S., Wei, S. J., Wang, T., and Ampuero, J. P.: Lower edge of locked Main Himalayan Thrust unzipped by the 2015 Gorkha earthquake, Nat. Geosci., 8, 708–711, doi:10.1038/NGEO2518, 2015.

Ayoub, F., Leprince, S., and Avouac, J. P.: Co-registration and correlation of aerial photographs for ground deformation measurements, ISPRS J. Photogramm., 64, 551–560, doi:10.1016/j.isprsjprs.2009.03.005, 2009.

Barnhart, W. D., Hayes, G. P., Briggs, R. W., Gold, R. D., and Bilham, R.: Ball-and-socket tectonic rotation during the 2013 M_w 7.7 Balochistan earthquake, Earth Planet. Sc. Lett., 403, 210–216, doi:10.1016/j.epsl.2014.07.001, 2014.

Barnhart, W. D., Briggs, R. W., Reitman, N. G., Gold, R. D., and Hayes, G. P.: Evidence for slip partitioning and bimodal slip behavior on a single fault: Surface slip characteristics of the 2013 M_w 7.7 Balochistan, Pakistan earthquake, Earth Planet. Sc. Lett., 420, 1–11, doi:10.1016/j.epsl.2015.03.027, 2015.

Boshuizen, C., Mason, J., Klupar, P., and Spanhake, S.: Results from the Planet Labs flock constellation, Proceedings of the AIAA/USU Conference on Small Satellites, http://digitalcommons.usu.edu/smallsat/2014/PrivEnd/1/ (last access: 4 May 2017), 2014.

COMET: New Zealand earthquake, Centre for Observation and Modelling of Earthquakes, Volcanoes and Tectonics, http://comet.nerc.ac.uk (last access: 20 January 2017), 2016.

Copernicus: ESA/EC Copernicus Sentinels Scientific Data Hub, https://scihub.copernicus.eu/, last access: 8 May 2017.

Debella-Gilo, M. and Kääb, A.: Sub-pixel precision image matching for measuring surface displacements on mass movements using normalized cross-correlation, Remote Sens. Environ., 115, 130–142, doi:10.1016/j.rse.2010.08.012, 2011a.

Debella-Gilo, M. and Kääb, A.: Locally adaptive template sizes in matching repeat images of Earth surface mass movements, IS-

PRS J. Photogramm., 69, 10–28, doi:10.1016/j.rse.2010.08.012, 2011b.

Dehecq, A., Gourmelen, N., and Trouve, E.: Deriving large-scale glacier velocities from a complete satellite archive: Application to the Pamir-Karakoram-Himalaya, Remote Sens. Environ., 162, 55–66, doi:10.1016/j.rse.2015.01.031, 2015.

Dominguez, S., Avouac, J. P., and Michel, R.: Horizontal coseismic deformation of the 1999 Chi-Chi earthquake measured from SPOT satellite images: Implications for the seismic cycle along the western foothills of central Taiwan, J. Geophys. Res.-Sol. Ea., 108, 2083, doi:10.1029/2001jb000951, 2003.

Earthexplorer: US Geological Survey Earthexplorer, http://earthexplorer.usgs.gov/, last access: 8 May 2017.

Fialko, Y., Simons, M., and Agnew, D.: The complete (3-D) surface displacement field in the epicentral area of the 1999 M_{W} 7.1 Hector Mine earthquake, California, from space geodetic observations, Geophys Res Lett, 28, 3063–3066, doi:10.1029/2001gl013174, 2001.

Foster, C., Hallam, H., and Mason, J.: Orbit determination and differential-drag control of Planet Labs cubesat constellation, AIAA Astrodynamics Specialist Conference in Vale, CO, August 2015, https://arxiv.org/pdf/1509.03270.pdf (last access: 4 May 2017), 2015.

GeoNET: New Zealand Earthquake Commission and GNS Science, http://info.geonet.org.nz/blog/quake (last access: 20 January 2017), 2016.

Girod, L., Nuth, C., and Kääb, A.: Improvemement of DEM generation from ASTER images using satellite jitter estimation and open source implementation The International Archives of the Photogrammetry, Remote Sensing and Spatial Information Sciences, XL-1/W5, 2015.

Kargel, J. S., Leonard, G. J., Shugar, D. H., Haritashya, U. K., Bevington, A., Fielding, E. J., Fujita, K., Geertsema, M., Miles, E. S., Steiner, J., Anderson, E., Bajracharya, S., Bawden, G. W., Breashears, D. F., Byers, A., Collins, B., Dhital, M. R., Donnellan, A., Evans, T. L., Geai, M. L., Glasscoe, M. T., Green, D., Gurung, D. R., Heijenk, R., Hilborn, A., Hudnut, K., Huyck, C., Immerzeel, W. W., Jiang, L. M., Jibson, R., Kaab, A., Khanal, N. R., Kirschbaum, D., Kraaijenbrink, P. D. A., Lamsal, D., Liu, S. Y., Lv, M. Y., McKinney, D., Nahirnick, N. K., Nan, Z. T., Ojha, S., Olsenholler, J., Painter, T. H., Pleasants, M., Pratima, K. C., Yuan, Q. I., Raup, B. H., Regmi, D., Rounce, D. R., Sakai, A., Donghui, S., Shea, J. M., Shrestha, A. B., Shukla, A., Stumm, D., van der Kooij, M., Voss, K., Xin, W., Weihs, B., Wolfe, D., Wu, L. Z., Yao, X. J., Yoder, M. R., and Young, N.: Geomorphic and geologic controls of geohazards induced by Nepal's 2015 Gorkha earthquake, Science, 351, aac8353, doi:10.1126/science.aac8353, 2016.

Kääb, A.: Correlation Image Analysis software (CIAS), http://www.mn.uio.no/icemass (last access: 20 January 2017), 2014.

Kääb, A. and Vollmer, M.: Surface geometry, thickness changes and flow fields on creeping mountain permafrost: automatic extraction by digital image analysis, Permafrost Periglac. 11, 315–326, doi:10.1002/1099-1530(200012)11:4>315::Aid-Ppp365>3.0.Co;2-J, 2000.

Kääb, A., Lamare, M., and Abrams, M.: River ice flux and water velocities along a 600 km-long reach of Lena River, Siberia, from satellite stereo, Hydrol. Earth Syst. Sci., 17, 4671–4683, doi:10.5194/hess-17-4671-2013, 2013.

Kääb, A., Winsvold, S. H., Altena, B., Nuth, C., Nagler, T., and Wuite, J.: Glacier remote sensing using Sentinel-2. Part I: radiometric and geometric performance, and application to ice velocity, Remote Sens., 8, 598, doi:10.3390/Rs8070598, 2016.

Konca, A. O., Leprince, S., Avouac, J. P., and Helmberger, D. V.: Rupture process of the 1999 M_{W} 7.1 Duzce earthquake from joint analysis of SPOT, GPS, InSAR, strong-motion, and teleseismic data: a supershear rupture with variable rupture velocity, B. Seismol. Soc. Am., 100, 267–288, 2010.

Leprince, S., Barbot, S., Ayoub, F., and Avouac, J. P.: Automatic and precise orthorectification, coregistration, and subpixel correlation of satellite images, application to ground deformation measurements, IEEE T. Geosci Remote, 45, 1529–1558, doi:10.1109/Tgrs.2006.888937, 2007.

Liu, J. G., Mason, P. J., and Ma, J. M.: Measurement of the left-lateral displacement of M_S 8.1 Kunlun earthquake on 14 November 2001 using Landsat-7 ETM + imagery, Int. J. Remote Sens., 27, 1875–1891, doi:10.1080/01431160500292023, 2006.

Marshall, W. and Boshuizen, C.: Planet Labs' remote sensing satellite system, Proceedings of the AIAA/USU Conference on Small Satellites, http://digitalcommons.usu.edu/smallsat/2013/all2013/7/ (last access: 4 May 2017), 2013.

Massonnet, D. and Feigl, K. L.: Radar interferometry and its application to changes in the earth's surface, Rev. Geophys., 36, 441–500, doi:10.1029/97rg03139, 1998.

Michel, R. and Avouac, J. P.: Coseismic surface deformation from air photos: The Kickapoo step over in the 1992 Landers rupture, J. Geophys. Res.-Sol. Ea., 111, B03408, doi:10.1029/2005jb003776, 2006.

Michel, R. and Rignot, E.: Flow of Moreno Glaciar, Argentina, from repeat-pass Shuttle Imaging Radar images: comparison of the phase correlation method with radar interferometry, J. Glaciol., 45, 93–100, 1999.

Michel, R., Avouac, J. P., and Taboury, J.: Measuring ground displacements from SAR amplitude images: application to the Landers earthquake, Geophys. Res. Lett., 26, 875–878, doi:10.1029/1999gl900138, 1999.

Nuth, C. and Kääb, A.: Co-registration and bias corrections of satellite elevation data sets for quantifying glacier thickness change, The Cryosphere, 5, 271–290, doi:10.5194/tc-5-271-2011, 2011.

Sciencealert: New Zealand's earthquake was so intense, it lifted the sea bed 2 metres above ground, http://www.sciencealert.com/new-zealand-s-earthquake-was-so-powerful (last access: 20 January 2017), 2016.

Singleton, A., Li, Z., Hoey, T., and Muller, J. P.: Evaluating subpixel offset techniques as an alternative to D-InSAR for monitoring episodic landslide movements in vegetated terrain, Remote Sens. Environ., 147, 133–144, doi:10.1016/j.rse.2014.03.003, 2014.

Stumpf, A., Malet, J. P., Allemand, P., and Ulrich, P.: Surface reconstruction and landslide displacement measurements with Pleiades satellite images, ISPRS J. Photogramm., 95, 1–12, doi:10.1016/j.isprsjprs.2014.05.008, 2014.

Stumpf, A., Malet, J.-P., and Delacourt, C.: Correlation of satellite image time-series for the detection and monitoring of slow-moving landslides, Remote Sens. Environ., 189, 40–55, doi:10.1016/j.rse.2016.11.007, 2017.

Planet Team: Planet Application Program Interface: In Space for Life on Earth. San Francisco, CA, https://api.planet.com (last access: 4 May 2017), 2016.

USGS Earthquake Hazard Program: M 7.8 – 54 km NNE of Amberley, New Zealand, http://earthquake.usgs.gov/earthquakes/ (last access: 20 January 2017), 2016.

Wang, T. and Jonsson, S.: Improved SAR amplitude image offset measurements for deriving three-dimensional coseismic displacements, IEEE J.-Stars, 8, 3271–3278, doi:10.1109/Jstars.2014.2387865, 2015.

Zhou, Y., Parsons, B., Elliott, J. R., Barisin, I., and Walker, R. T.: Assessing the ability of Pleiades stereo imagery to determine height changes in earthquakes: A case study for the El Mayor-Cucapah epicentral area, J. Geophys. Res.-Sol. Ea., 120, 8793–8808, doi:10.1002/2015JB012358, 2015.